# Models for sensing by nanowire networks: application to organic vapour detection by multiwall carbon nanotube—DNA films



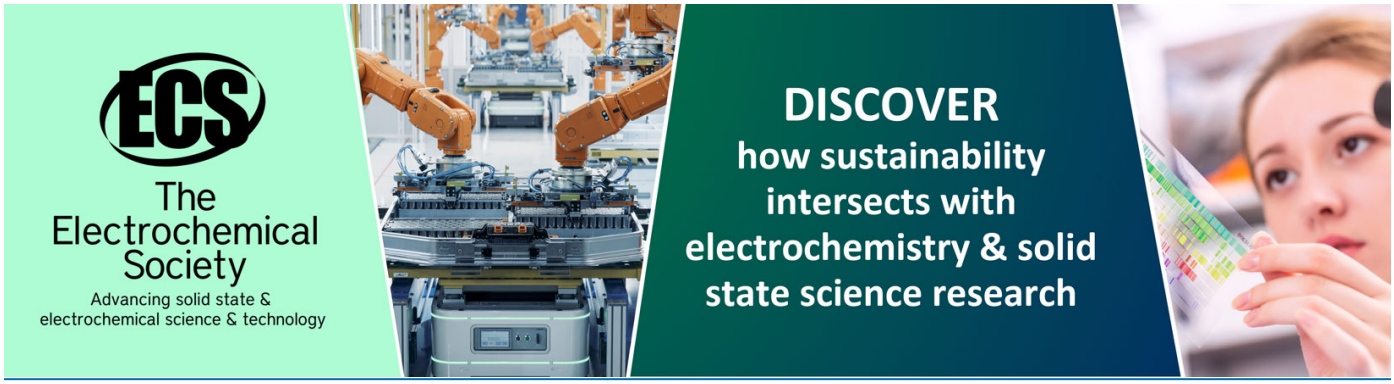

OPEN ACCESS
IOP Publishing
Nanotechnology

Nanotechnology **33** (2022) 045502 (15pp)
https://doi.org/10.1088/1361-6528/ac2e20

# Models for sensing by nanowire networks: application to organic vapour detection by multiwall carbon nanotube—DNA films

**Shams B Ali**[1,2], **Atsinafe B Oshido**[1,3], **Andrew Houlton**[1] and **Benjamin R Horrocks**[1]

[1] Chemical Nanoscience Laboratories, School of Natural and Environmental Sciences, Bedson Building, Newcastle University, Newcastle upon Tyne, NE1 7RU, United Kingdom
[2] Department of Laser and Optoelectronics Engineering, University of Technology, Baghdad, 10066, Iraq
[3] Department of Chemistry, Benue State University, Makurdi, 970222, Nigeria

E-mail: b.r.horrocks@ncl.ac.uk

Received 7 March 2021, revised 23 August 2021
Accepted for publication 8 October 2021
Published 8 November 2021

**Abstract**

Electronic sensors for volatile organic compounds have been prepared by drop-casting dispersions of multi-wall carbon nanotubes (MWCNTs) in aqueous solutions of $\lambda$-DNA onto Pt microband electrodes. The MWCNTs themselves show a metal-like temperature dependence of the conductance, but the conductance of DNA/MWCNT composites has an activated component that corresponds to inter-tube tunneling. The resistance of the composite was modelled by a series combination of a term linear in temperature for the nanotubes and a stretched exponential form for the inter-tube junctions. The resistance may increase or decrease with temperature according to the composition and may be tuned to be almost temperature-independent at 67% by mass of DNA. Upon exposure to organic vapours, the resistance of the composites increases and the time-dependence of this signal is consistent with diffusion of the vapour into the composite. The fractional change in resistance at steady-state provides an analytical signal with a linear calibration and the presence of DNA enhances the signal and adjusts the selectivity in favour of polar analytes. The temperature dependence of the signal is determined by the enthalpy of adsorption of the analyte in the inter-tube junctions and may be satisfactorily modelled using the Langmuir isotherm. Temperature and pressure-dependent studies indicate that neither charge injection by oxidation/reduction of the analyte nor condensation of analyte on the device is responsible for the signal. We suggest that the origin of the sensing response is an adsorption of the analyte in the inter-tube regions that modulates the tunneling barriers. This suggests a general route to tuning the selectivity of MWCNT gas sensors using non-conductive polymers of varying chemical functionality.

Keywords: nanotubes, DNA, sensing, volatile organics, conductance

(Some figures may appear in colour only in the online journal)

## 1. Introduction

Carbon nanotubes (CNTs) have been intensively studied because of their unusual electronic and mechanical properties [1, 2]. They have large coherence lengths and, depending on how the graphene sheet is rolled to form a tube, single-wall carbon nanotubes (SWCNTs) may have semiconducting or metallic conductivity. Multi-wall carbon nanotubes (MWCNTs), in which a single sheet is wound in the form of a scroll or multiple nanotubes are arranged in a concentric manner, are generally metal-like. Owing to their large surface-to-volume ratio, CNTs have been extensively investigated as electrical transducers for use in chemical sensing [3–5]. Indeed, an early

application of nanotubes was in a chemical sensor for $NO_2$ and $NH_3$ [6].

CNTs are attractive in gas sensing applications because simple two or three terminal electronic devices [7, 8] can be used directly as sensors [9]. The simplest nanotube sensor is a 2-terminal device in which the current flows through CNTs between source and drain contacts and is modulated by the presence of the analyte on the nanotube surface. The high aspect ratio of CNTs means that a large fraction of the atoms lie on the surface (100% in the case of SWCNTs). In principle their conductance should therefore be extremely sensitive to the local chemical environment. Devices may be constructed from single CNTs or networks [10]. Single CNT devices offer good sensitivity and are simpler to model, but they are not robust. Devices prepared from networks of CNTs have the advantage of more straightforward fabrication and are less fragile, but the conduction pathway is more complex [5]. Three-terminal devices, with an additional gate electrode, provide more detailed information for understanding the electron transport [11], but the 2-terminal devices are suitable as low-cost distributed sensors.

The mechanism of operation of CNT-based sensors is incompletely understood and an active topic of investigation [5]. There are many possible sensing mechanisms, including intra and inter CNT phenomena [10, 12]. Intra-tube mechanisms are typically charge injection by the analyte leading to an increase or a decrease in the carrier density [6] or changes in the surface scattering rate produced by adsorption of analytes on the surface [13]. However the current in typical devices may be limited by factors other than the conductance of CNTs themselves; a Schottky barrier may exist at the SWCNT-metal contact electrode or there may be substantial tunneling barriers between individual CNTs [14]. Even in simple sensors, the mechanism of sensing may be complex because the analyte may act on the nanotubes themselves, at the metal contact/nanotube junctions or at inter-tube junctions. The effect of oxidising or reducing analytes on SWCNTs is often attributed to charge transfer between the analyte and the nanotubes, but changes in carrier mobility due to surface scattering may also occur. Intratube effects are more important for defective or less conductive CNTs [15], therefore it is expected that inter-tube effects will be more important for devices based on metal-like MWCNTs [16, 17].

The selectivity of sensors based on bare CNTs can be improved by functionalisation [18, 19] and polymer coating [20]. Coating with polymers is a common technique because, unlike covalent functionalisation, it does not disrupt the $\pi$-system of the nanotubes [5]. DNA is a convenient polyelectrolyte for aqueous solubilisation of CNTs [21, 22]. Most reports utilise single-stranded DNA for this purpose, but double-stranded DNA has also been used to prepare thin film transistors [23], transparent conductive films [24] and modified electrodes [25]. Sensors based on DNA-decorated CNTs have been demonstrated for hybridisation [26] and for organic vapours [27–30]. These have mainly utilized SWCNTs and single-stranded DNA. The response may be governed by the work function at the CNT/contact [26] or by depletion of the hole density [28]. In this work we prepare double-stranded DNA/MWCNT composites by drop-casting onto microband electrodes (MBEs) from aqueous dispersions of MWCNTs in $\lambda$-DNA solutions. These devices are investigated as sensors for volatile organic compounds (VOCs) and the mechanism of the sensing response is probed using temperature-dependent measurements of their conductivity and sensing response.

We show that MWCNT-dsDNA composites (denoted DNA/MWCNT below) have superior sensitivity to bare MWCNT networks for the detection of a range of VOCs. The choice of dsDNA to prepare such composites with CNTs is motivated by the well-known strong interaction of polyelectrolytes with CNTs and not by the biochemical properties of DNA. This interaction facilitates the preparation of devices by a simple drop-casting approach. The role of the DNA is to reduce the conductance of the composite compared to bare CNTs and enhance the contribution of inter-tube barriers to the resistance of the network. Adsorption of various VOCs in the composite modulates these barriers and produces a useful analytical signal. We provide evidence for the contribution of such tunneling barriers from the temperature dependence of the steady-state current–voltage curves. Finally, the temperature-dependence of the analytical response is analysed in terms of the van't Hoff equation for an adsorption process; we conclude that adsorption of the VOCs rather than charge injection is responsible for the signal and that the origin of the response lies at the inter-tube junctions.

## 2. Experimental

### 2.1. Reagents

Lambda DNA (N3011, 500 $\mu$g ml$^{-1}$ denoted $\lambda$-DNA below) was purchased from New England Biolabs (Hitchin, UK). The phage is isolated from the heat-inducible lysogen E.coli l cI857 S7. The DNA is isolated from the purified phage by phenol extraction and dialyzed against 10 mM Tris-HCl (pH 8.0) + 1 mM EDTA. $\lambda$-DNA comprises 48 502 base pairs [31] and the molar mass estimated from the supplier's data was $3.0 \times 10^6$ g mol$^{-1}$.

MWCNTs (Elicarb$^{TM}$ P940, denoted MWCNT below) were purchased from Thomas Swan (Consett, UK). The MWCNTs were specified as having a mean diameter in the range 10–12 nm and a maximum metal oxide content of 5 wt%.

The solvents methanol, acetone and ethanol were purchased from Fisher Scientific Ltd (Loughborough, UK) while chloroform was obtained from Sigma–Aldrich Company Ltd (Gillingham, UK); all were used as received (>99% purity) without further purification. Silicon wafer, p-type, boron-doped, oriented ⟨111⟩, diameter (100 ± 0.3 mm) and resistivity (0.09–0.12 Ω cm) was purchased from Pi-KEM Ltd. Deionized water (with a nominal resistivity of 18.2 MΩ cm) from a Barnstead NANOpure® and DIamond$^{TM}$ reverse osmosis system was used throughout.

### 2.2. Preparation of DNA/MWCNT composites

A dispersion of MWCNTs was prepared by adding 0.1 mg of CNTs to 10 ml methanol. The solution was sonicated for 3 h at ambient temperature (15 °C) to ensure complete dispersion and to reduce agglomeration of the nanotubes (750 W Ultrasonic Processor + microtip at 20% amplitude, Sonics & Materials). The DNA/MWCNT dispersions were prepared by adding 2 $\mu$l, 5 $\mu$l or 10 $\mu$l of $\lambda$-DNA to 50 $\mu$l of the methanolic dispersion of MWCNTs. The mixture was sonicated for about 5 min and then allowed to stand overnight. The resultant mixture forms a dispersion after sonication. The mole fractions of DNA (moles of base pairs, moles of carbon atoms in MWCNTs) in the dispersions and the composites prepared by drop-casting were 0%, 3.1%, 7.4% and 13.8% respectively. The corresponding mass fractions of DNA are 0%, 67%, 83% and 91%. Each dispersion was sonicated briefly before drop-casting in order to ensure a homogenous DNA/CNT film.

### 2.3. X-ray photoelectron spectroscopy

A Thermo Scientific K-Alpha photoelectron spectrometer equipped with a monochromatic Al K$\alpha$ x-ray excitation source (1486.7 eV) was used to collect photoemission spectra (NEXUS, Newcastle University). The operating power was 72 W (12 kV, 6 mA) and the chamber pressure was $\simeq 3 \times 10^{-9}$ Torr. The photoelectrons were filtered by a hemispherical analyzer and recorded by multichannel detectors. High resolution spectra were recorded with a step size of 0.1 eV and the survey scan had a step size of 0.4 eV. The pass energies were 150 eV (survey scan) and 40 eV (high resolution scans). The binding energies obtained in the XPS analysis were calibrated using the lowest C 1s component (284.8 eV) as a reference. Spectral peaks were fitted using the CasaXPS software version 2.3.24 from Casa Software Ltd (Teignmouth, UK) [32]. A U 2 Tougaard background and the LA(1.53, 243) line shape were used for fitting. Samples were prepared by drop-casting $\simeq 20$ $\mu$l DNA/MWCNT dispersion (91% DNA by mass) onto clean p-Si(100) chips.

### 2.4. Atomic force microscopy

Atomic force microscopy images were obtained using the ScanAsyst-in-Air mode of a Multimode VIII AFM coupled to a Nanoscope V controller (Bruker) and an "E" scanner. Nanoscope software version 9.1 was used to acquire the images. Silicon nitride cantilevers (ScanAsyst, Bruker) were used for imaging. These cantilevers have a spring constant of 0.7 N m$^{-1}$ and a resonance frequency of 150 kHz with a nominal tip radius of about 2 nm. The acoustic and vibrational noise of the microscope was reduced by placing it on an acoustic enclosure/isolation table. Image analysis was performed with Nanoscope analysis software (version 1.5).

### 2.5. Transmission and scanning electron microscopy (SEM)

Samples of MWCNTs were prepared for transmission electron microscopy (TEM) by drop-casting 3 $\mu$l of a dispersion in chloroform onto a holey carbon grid. The images were obtained using a JEOL 2100F transmission electron microscope operating at 200 kV (University of Durham, GJ Russell Electron Microscopy Facility).

Samples of DNA/MWCNTs (91% by mass DNA) for SEM were prepared by drop-casting $\simeq$20 $\mu$l of the DNA/MWCNT onto clean p-Si(100) chips. The SEM instrument was a JEOL JSM-5610LV operated at 20 kV and images were taken using the secondary electron detector (Electron Microscopy and Analysis Unit at SAgE Analytical, Newcastle University).

### 2.6. FTIR

An IRAffinity-1S Fourier transform infrared spectrophotometer (Shimadzu) operating at 8 cm$^{-1}$ spectral resolution and equipped with a DLATGS detector was used to record spectra in the range of wavenumbers from 400 to 4000 cm$^{-1}$. Thirty-two scans were co-added and averaged. The sample was prepared by drop-casting 5 $\mu$l of the DNA/CNT dispersion on a single reflection diamond ATR accessory (Quest Specac®, Supelco).

### 2.7. Raman spectroscopy

Raman spectra were obtained using a confocal microscope (CRM200, Witec GmbH, Ulm, Germany). A diode laser of 60 mW output power at a wavelength of 488 nm was coupled to the microscope via a single mode optical fiber and provided the excitation light. The microscope is fitted with a Raman edge filter (OD = 6) to attenuate the elastically-scattered light. The backscattered light was collected by a multimode fiber which served as the confocal pinhole and dispersed on a grating (600 lines mm$^{-1}$). Spectra were acquired using a Peltier-cooled CCD detector.

### 2.8. Electrodes

Platinum MBEs (Smart Microsystems Pt MB-4000, Windsor Scientific Ltd. Slough, UK) were used to fabricate electronic devices for two-terminal electrical characterisation of DNA/MWCNT films and vapor sensing experiments. The MBEs were fabricated on $Si/SiO_2$ substrates. Four independent platinum electrodes were patterned on the top of the $SiO_2$ layer. The platinum MBEs were cleaned by rinsing with ethanol and dried in a stream of nitrogen gas. The height of the electrodes is 200 nm and their width is 10 $\mu$m with 10 $\mu$m spaces between them. The surface of the MBEs was electrically insulated except for a window, 2 mm in length, on which the DNA/MWCNT film was deposited by micropipette. Devices were fabricated by drop-casting 3 $\mu$l of the DNA/MWCNT dispersion onto the platinum MBEs. During sensing experiments, electrical contact was made between neighbouring electrodes. During current–voltage characterisation, the bias was applied between next-nearest neighbour electrodes.

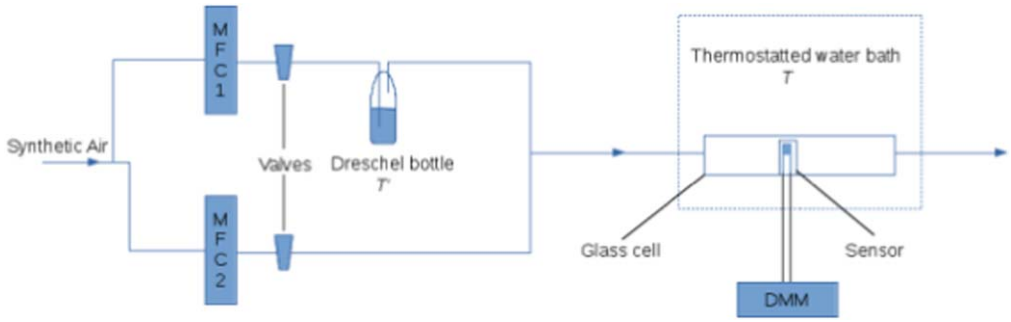


**Figure 1.** Block diagram of the sensing apparatus. The temperature of the Dreschel bottle ($T'$) was monitored by a thermocouple. The temperature of the sensing cell was controlled by a thermostatted water bath ($T$).

### *2.9. Current–voltage characterisation*

Two-terminal current–voltage measurements at different temperatures were performed on a probe station (Cascade Microtech with a B1500A parameter analyser, Agilent) using a thermal chuck system (Model ETC–200L, ESPEC, Japan). All the electrical characterisation was carried out under dry nitrogen in the absence of illumination. The clean platinum MBEs were analysed on the probe station and reference current–voltage curves were recorded which showed the background currents to be less than 100 fA at 2 V applied bias.

The DNA/MWCNT composite was deposited onto the Pt microbands by drop casting and the droplet (3 $\mu$l) was carefully combed across the exposed area by dragging it with the tip of a pipette. The electrodes were the kept in a laminar flow hood (Envair Ltd, York, UK) at room temperature to facilitate drying of the solution in a low-dust environment. The sample was transferred to the chamber of the probe station chamber and maintained under dry nitrogen for 30 min before collecting the current–voltage curves.

### *2.10. Gas sensing*

DNA/MWCNT dispersions were drop-cast as films on MBEs and the interelectrode resistance was measured using a standard DMM (Agilent 34 401A). The sensing response is defined as $S = (R - R_0)/R_0 \times 100\%$ where $R_0$ is the resistance in a synthetic air atmosphere and $R$ is the resistance at steady-state after exposure to an air/analyte mixture. A simple LabVIEW program was used to record the resistance against time.

The atmosphere at the sensor was controlled by mixing gas streams; one of pure synthetic air and a second of synthetic air saturated with the vapour of the analyte (VOC = volatile organic compound). Figure 1 is a block diagram of the apparatus. Synthetic air (Zero air 270 020-V, BOC Ltd, ) is prepared by mixing pure oxygen and nitrogen in a 1:4 ratio and has a much lower level of impurities than ambient air (hydrocarbons $< 0.1$ vpm; $CO_2 < 1$ vpm; $H_2O < 2$ vpm and $NO_x < 0.1$ vpm). Digital mass flow controllers (Brooks Instrument 5850S, PA, USA) and the Brooks 0260 Smart Interface and software were used to independently control the volume flow rates of the two gas streams. The mass flow controllers have a settling time of $\simeq$1 s that is much shorter than the 90% response time of the sensors, which is of the order of $10^2$ s. The sensor test system also comprised 6 mm id PVC tubing and manual valves to deliver the gas to the sensors inside a locally-constructed glass vessel. The temperature of the sensor was controlled by immersing the glass vessel in a digitally-controlled water bath (Grant TX150, Wolf Laboratories Ltd, UK).

The flow of pure synthetic air was fixed at 125 ml min$^{-1}$ and the volume flow rate through the Dreschel bottle was varied between 125 and 500 ml min$^{-1}$. A thermocouple was used to monitor the temperature of the Dreschel bottle ($T'$) in order to determine the saturated vapour pressure of the VOC from available data tables (NIST WebBook [33]). The temperature $T'$ was not varied during the experiments. The temperature at the sensor ($T$) was monitored by a separate thermocouple. This temperature was varied using the water bath in order to carry out the temperature-dependent studies of the sensing mechanism.

## 3. Results and discussion

First we discuss the structure and composition of the composites, then we describe the electrical behaviour of the DNA/MWCNT composites and finally we investigate the sensing response of two-terminal devices based on DNA/MWCNT films. DNA is not itself an electronic conductor over mesoscopic lengths [34–37]. However it is well-known to be useful for the dispersion of CNTs in aqueous media, because it interacts strongly with the tube walls and stabilises the dispersion by electrostatic means; other polyelectrolytes have similar effects [38]. DNA also affects the sensing behaviour of CNT devices towards organic vapours [27].

### *3.1. Structure and composition*

Figure 2 shows transmission electron microscope images of the MWCNTs used in this work. The MWCNTs have the 'Russian doll' structure which is usually associated with a metal-like conductance behaviour.

The composition of the DNA/MWCNT films was analysed by x-ray photoelectron spectroscopy. The expected elements C, N, O, P and Na were detected and the corresponding spectra are shown in figure 3. The C 1s spectrum was

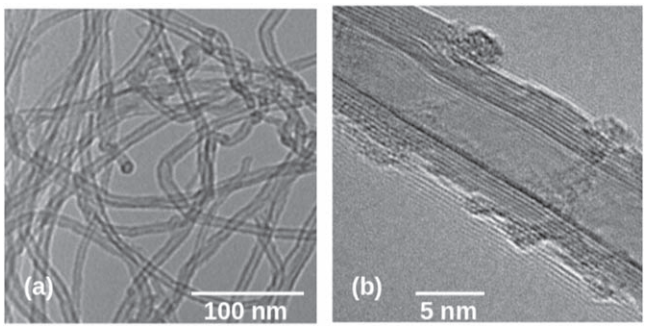


**Figure 2.** TEM images of (a) bare MWCNTs and (b) a single MWCNT at higher resolution showing the Russian doll structure.

fitted with 4 components and the energy scale calibrated such that the largest component (C–C) was at a binding energy of 284.8 eV. Higher energy components at 286.2 and 288.5 eV are typical of C–O and C=O moieties in DNA and, possibly, oxidised nanotubes. A fourth, minor component at 284.3 eV was necessary to model the low binding energy side of the main C 1s feature. This is close to the value of 284.45 reported for untreated MWCNTs [39], however it is not possible to assign this definitively to MWCNTs. There is evidence of a broad, weak plasmon peak, attributable to CNTs [40, 41], just below 310 eV in figure 3. However, the clearest spectroscopic evidence for the MWCNTs in the samples is obtained from Raman spectroscopy below.

The N 1s spectrum was fitted with components at 401.4 eV (amine, $–NH_2$) and 399.5 eV (–NH–, –N=). The amine component at 401.4 eV comprised 16.5% of the nitrogen atoms and the lower energy component due to imines accounted for the bulk, 84.5% of the nitrogen atoms. This ratio is consistent with that expected for DNA [42]. The O 1s spectrum was fitted with components at 530.9, 532.2 and 532.6. The third, minor component at 532.6 eV was necessary to model the high binding energy side of the O 1s spectrum. We assign these features to a combination of adsorbed water and oxygen functionalities in DNA [43]. The P 2p spectrum was satisfactorily modelled by a single component at a binding energy of 133.9 eV because the spin–orbit coupling was not resolved. This binding energy is characteristic of the phosphate groups expected for a sample containing DNA and together with the N 1s spectrum is robust evidence of the presence of DNA that is not subject to uncertainty arising from contamination by adventitious carbon [43]. Finally, the survey spectrum showed the presence of $Na^+$ (DNA countercations) with a single component at 1071.5 eV corresponding to the binding energy of Na 1s electrons.

The DNA/MWCNT film structure was investigated by SEM and atomic force microscopy. Figure 4 shows an electron micrograph of the same film analysed by photoelectron spectroscopy with 91% DNA by mass. The film takes the form of a dense fibrous network. DNA molecules are not visible at the resolution of SEM, however, the image shows bundles of CNTs which were explored further by atomic force microscopy.

Figure 5 shows AFM images of bare MWCNTs and a DNA/MWCNT composite drop-cast on Si chips, dried and imaged in air. The DNA/MWCNT composite has a mole fraction of 3.1% on the basis of base pairs and nanotube carbon atoms. The fraction of DNA by mass is 67%. The bare MWCNTs are visible as a tangled mass of fibres in figure 5(a). After coating with DNA, the AFM image suggests clumping of individual nanotubes and DNA strands into thicker features (figure 5(b)). Cross-section profiles of the two samples are shown in figure 5(c) for MWCNTs and figure 5(d) for the 67% DNA/MWCNT composite. The profile in (d) shows significantly broader features, which we attribute to a bundling of the fibers in the sample. The difference between these samples provides indirect evidence for an interaction between DNA molecules and MWCNTs in the DNA/MWCNT composite.

In order to further investigate the nature of the DNA–MWCNT interaction, we employed vibrational spectroscopies which are sensitive to the chemical structure of these materials. Figure 6 presents Raman spectra for drop-cast samples of MWCNTs, $\lambda$-DNA and DNA/MWCNTs. The DNA/MWCNT composite has a mole fraction of 13.8% on the basis of base pairs and nanotube carbon atoms (91% by mass DNA). As expected, the spectrum of samples containing MWCNTs shows two main peaks at 1370 and 1594 $cm^{-1}$ for the well-known D and G bands of CNTs. The Raman spectrum of $\lambda$-DNA is dominated by a strong peak at 813 $cm^{-1}$ which is assigned to the symmetric stretching mode of the phosphodiester backbone [44, 45]. After preparation of DNA/MWCNTs composites, this peak remains, but is lower in intensity than expected on the basis of the mass fraction of DNA in the composite and shifted to 800 $cm^{-1}$. The shift can be rationalised on the basis of the interaction of the charged phosphate groups with the metal-like nanotubes and suggests the composite is not merely a mixture of weakly-interacting components. Figure 7 compares the FTIR spectrum of $\lambda$-DNA and the difference spectrum for the composite DNA/MWCNTs and bare MWCNTs in order to observe the differences between the environments of the DNA molecules in the composite and in $\lambda$-DNA. The positions of the bands in the 1400–1600 $cm^{-1}$ region are similar [46–48]; these include the in-plane modes of the nucleobases (1548, 1552 $cm^{-1}$ DNA, composite) and C–N/ring modes (1474, 1464 $cm^{-1}$ DNA, composite). There are differences in the C=N and C=O stretches (1631, 1660 $cm^{-1}$ DNA, difference), but this region is known also to include contributions from bound water and the data suggests partial dehydration in the composite. The main differences observed are in the intensity of the symmetric P–O stretch of the phosphate (1069, 1074 $cm^{-1}$ DNA, difference) and of the sugar-phosphate stretching mode (1159, 1159 $cm^{-1}$ DNA, difference) indicated by the dotted lines in figure 7. This suggests screening of the transition dipole by the metal-like nanotubes. The modes associated with the nucleobases are not as strongly affected as the modes associated with the phosphate backbone. This is likely to occur because the former are internal to the DNA double helix and not in close contact with the nanotubes. The data are consistent with an interaction of the DNA with the nanotubes via the charged phosphate groups.

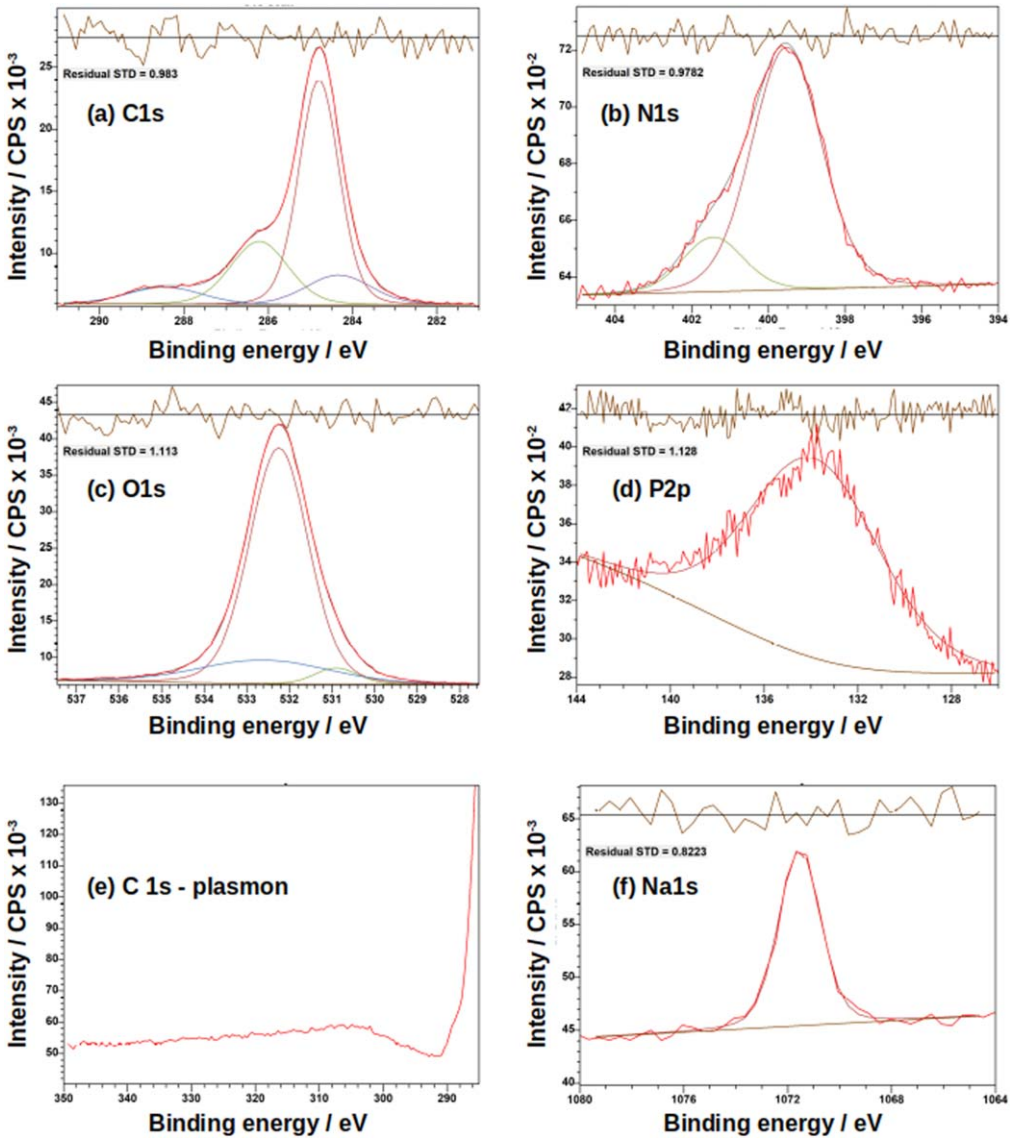


**Figure 3.** X-ray photoelectron spectra of DNA/MWCNT at 91% by mass of DNA. The sample was drop cast on a p-Si(100) substrate. The experimental data is the red curve and the rest are fitted components. The residual of the fit is shown at the top of each panel. (a) C 1s spectrum; (b) N 1s spectrum; (c) O 1s spectrum; (d) P 2p spectrum; (e) C 1s region showing evidence of a plasmon peak near 310 eV and (f) Na 1s region of a survey spectrum.

### *3.2. Electrical characterisation*

Prior to the sensing experiments, we characterised the electrical properties of the composites using two terminal current–voltage measurements. Devices were prepared by drop-casting dispersions of DNA/MWCNT onto Pt-on-$SiO_2$/Si MBEs. Samples of CNTs in the absence of DNA—bare MWCNTs—were prepared similarly and used as controls. Current–voltage ($IV$) curves were recorded on a probe station under a dry nitrogen atmosphere in the absence of illumination and at a controlled temperature. Ohmic $IV$ curves were observed over the range $-2.0\ \text{V} > V_{\text{applied}} < 2.0\ \text{V}$ in all cases and the differential conductance at zero bias was extracted by linear regression. Figure 8 summarises the variation of differential conductance with temperature for all the DNA/MWCNT composites studied. The bare MWCNT device shows a decrease in conductance as the temperature increases, which is typical of the metal-like behaviour of MWCNTs [1]. However, as the ratio of DNA:CNTs is increased, the gradient of the Arrhenius plot decreases and changes sign; for DNA mass fractions $> 67\%$ (mole fractions $> 3.1\%$) the conductance increases with temperature. It is also worth noting that the conductance of the devices decreases monotonically as the fraction of DNA increases.

The data of figure 8 can be understood in terms of a simple model in which the metal-like temperature dependence of the multi-wall nanotube conductivity is combined with an activated process assigned to inter-tube hopping. We model the electrical properties of DNA/MWCNT composites as a network of ohmic resistances (the nanotubes) and tunnel junctions where the carriers hop between nanotubes. We are primarily interested in the qualitative aspects of the temperature-dependence of the network conductance and therefore choose a stretched exponential form for the resistance of the

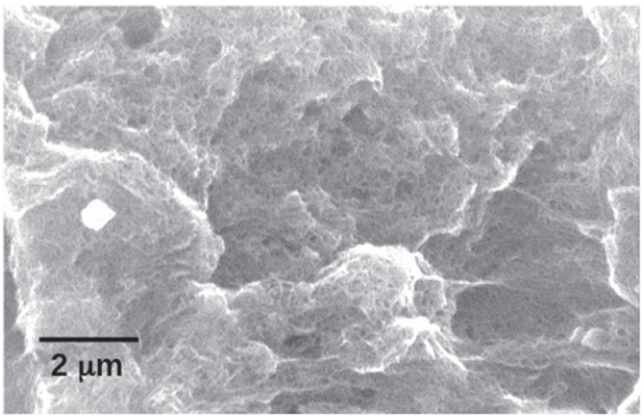


**Figure 4.** Scanning electron micrograph of a DNA/MWCNT film. The sample was 91% DNA by mass and drop-cast on an Si chip.

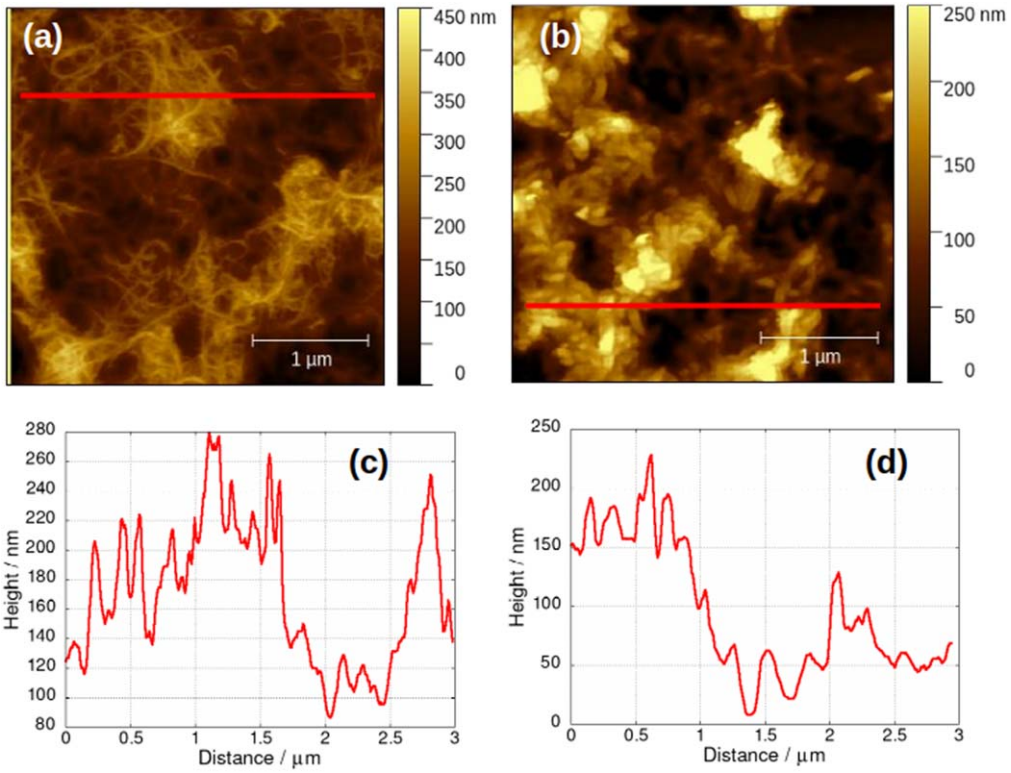


**Figure 5.** AFM images of (a) MWCNTs and (b) DNA/MWCNT (67% DNA by mass). The samples were prepared by drop-casting onto Si(111) chips and imaged in air. Height profiles along the red lines marked on (a) and (b) are shown in parts (c) and (d) respectively.

inter-tube junctions ($R_j$) given by equation (1).

$$R_j = R_j^0 \exp\left(\frac{T_0}{T}\right)^{\beta}. \tag{1}$$

$R_j^0$ and $T_0$ are constants that can be determined by a regression analysis of the experimental data. We take $\beta = \frac{1}{2}$ and treat the DNA/MWCNT composite as if it were similar to a granular metal [49]. The nanotubes make a substantial contribution to the resistance at low DNA:CNT ratios and we model their temperature dependence with a simple linear function appropriate for a metal given by equation (2)

$$R_m = a + bT. \tag{2}$$

The overall network resistance is assumed to be well-approximated as a series combination of equations (1) and (2) and the conductance is therefore given by equation (3)

$$G = (R_j + R_m)^{-1}. \tag{3}$$

Figure 8 also shows the fit to the data of the regression model defined by equations (1)–(3). The extracted values of $T_0$ and the corresponding activation energies $E_0 = k_B T_0$ are collected in table 1. The fit of the model to the data is satisfactory. However, at the highest loading with DNA (91%), a deviation from the model is observed in which the conductance becomes temperature-independent when $1000/T \gtrsim 3$.

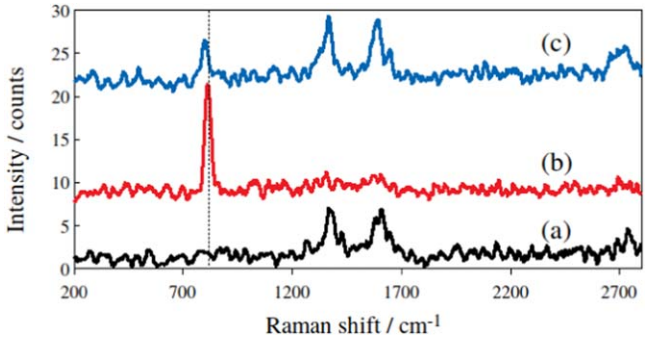


**Figure 6.** Raman spectra of MWCNTs, $\lambda$-DNA and a composite drop-cast on glass coverslips. (a) MWCNTs, (b) $\lambda$-DNA and (c) DNA/MWCNT composite, which was 91% $\lambda$-DNA on a mass fraction basis. The dotted line indicates the 813 $cm^{-1}$ band in DNA discussed in the text. The laser wavelength was 488 nm and the back-scattered light was dispersed on a grating with 600 lines $mm^{-1}$. The spectra are offset on the intensity axis for clarity.

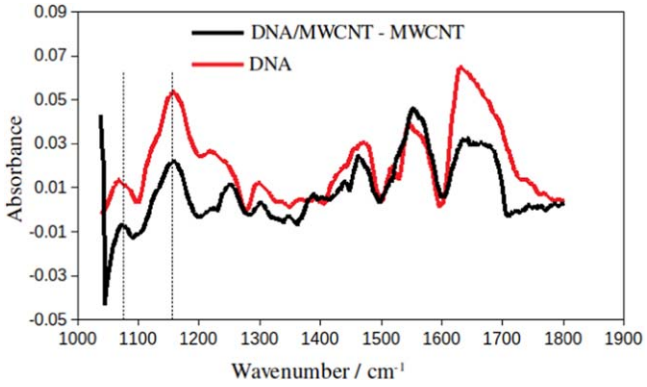


**Figure 7.** FTIR spectra. The fingerprint region of the $\lambda$-DNA spectrum (red line) and the difference spectrum (black line) for samples of DNA/MWCNT—MWCNT where the composite DNA/MWCNT was 91% DNA by mass. The resolution was 8 $cm^{-1}$ and 32 scans were co-added and averaged.

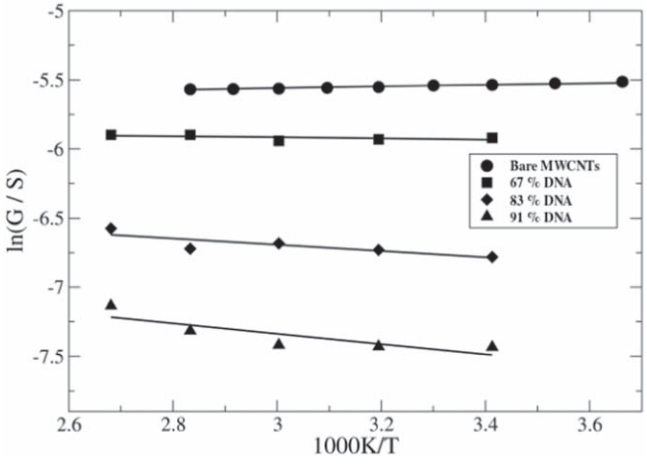


**Figure 8.** Arrhenius plot ($\ln G$ versus $1/T$) of the conductance $G$ of films of MWCNTs with and without DNA in varying ratios. The statistical errors on the datapoints were <1% in all cases.

**Table 1.** Activation energies $E_0 = k_B T_0$ and temperatures $T_0$ obtained from the least squares fitting of the regression model of equations (1)–(3) to the variation of differential conductance with temperature in figure 8. The uncertainties are standard errors estimated under the usual assumption of i.i.d. and normal measurement errors.

| DNA mass fraction | $E_0$/meV | $T_0$/K |
|---|---|---|
| 67% | $84.5 \pm 5.3$ | $980 \pm 61$ |
| 83% | $136 \pm 3.0$ | $1580 \pm 35$ |
| 91% | $223 \pm 3.1$ | $2590 \pm 36$ |

As the ratio of DNA:CNTs increases, the contribution of the junctions between tubes to the overall resistance is expected to increase because DNA coats the CNTs. In our model, this corresponds to an increase in the values of $R_j^0$ and $T_0$. If the contribution of the junctions between DNA-coated CNTs were to dominate, then $G \simeq 1/R_J$ and the temperature dependence of the resistance would have the stretched exponential form of equation (1) and the conductance would increase with increasing temperature. On the other hand, at low DNA:CNT mole ratios, when the CNT conductance dominates, the temperature dependence of the resistance is similar to that of a metal and the conductance decreases as the temperature increases as indicated by equation (2). These two factors are combined in equation (3) which describes the transition from the metallic conductance–temperature behaviour of bare MWCNTs to the stretched exponential behaviour typical of granular metals.

The data of table 1 shows that the average tunneling barrier increases monotonically as the mass fraction of DNA increases. This is useful for sensor design because it is possible to choose a mass fraction of DNA (67%) for which the device conductance is very weakly dependent on temperature and therefore the response to analytes can be more easily distinguished from temperature effects.

### *3.3. Sensing response time*

Synthetic air was used as the background in the sensing experiments. Two streams of air were mixed, one of which passed through a Dreschel bottle and was saturated with the analyte vapour as illustrated in figure 1. The partial pressure of the analyte, $p$, was controlled using mass flow controllers to set the volume flow rates of the two streams, denoted $V_{voc}$ and $V_{air}$ corresponding to the analyte and to pure, dry air.

$$p = p^* \frac{V_{voc}}{V_{air} + V_{voc}}. \tag{4}$$

$p^*$ is the saturated vapour pressure at the temperature of the Dreschel bottle. Upon switching the gas flow rates, an abrupt change in analyte concentration was produced and the time-response of the sensor was observed.

In order to investigate the interaction of the analyte with the sensor, the temperature, $T$, of the glass cell containing the sensor was controlled using a water bath. We use $T$ to indicate

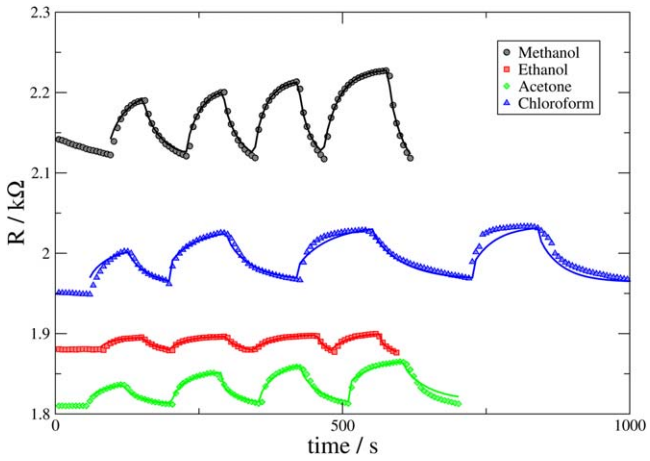


**Figure 9.** Representative examples of raw resistance data for exposure to pulses of analyte of increasing concentration ($p/p^*$=0.5, 0.67, 0.75, 0.8). The DNA/MWCNT composite was 67% by mass DNA and the sensor temperature was $T = 60$ °C. The solid lines are least squares fits to the data of equation (5) with the same time parameter $\tau$ for the analyte response and the recovery.

the sensor temperature throughout; this is distinct from the temperature of the Dreschel bottle $T'$. The latter is only required to determine $p^*$ and was constant during each experiment.

Figure 9 shows representative raw data of resistance against time for a DNA/MWCNT composite for each of the VOCs investigated. The stable value of the resistance in synthetic air is denoted $R_0$. Upon exposure to the analyte, the resistance increases and reaches an approximately steady value. Upon switching the flow back to synthetic air, the resistance decreases and eventually returns towards the baseline, although there is evidence of drift in the value of $R_0$, especially in the methanol data of figure 9. We exposed the sensor to a series of pulses of analyte of increasing concentration and 50–100 s duration. The time-independent steady state value of resistance in response to the *i*th pulse of analyte is denoted $R_0 + \Delta R_i$. The sensing response can, in principle, be modelled as transport-limited or kinetically-limited. We discuss both possibilities and then justify our preference for the transport-limited model in this particular case.

*3.3.1. A transport-limited model of the response time of the sensor.* The time-dependence of the resistance can be modelled in terms of the uptake of analyte by the composite. The uptake of analyte was treated as a Fickian diffusion process and the composite was modelled as a film of uniform thickness $L$ and analyte diffusion coefficient $D$. At the film/air interface, the analyte surface concentration is given by a step function: $c(L) = c_0$ for $t \geqslant 0 \text{and} c(L) = 0 \text{for} t < 0$. The initial condition is $c(z) = 0$ for $0 \leqslant z < L$ where $z$ is the coordinate in the direction normal to the film. The underlying glass substrate is impermeable, therefore a no-flux boundary condition is imposed at the substrate. Solution of the diffusion equation under these conditions and integration of the analyte concentration profile $c(z)$ over the thickness of the film results in equation (5) for the surface excess of analyte, $\Gamma(t)$, taken up by the film

$$\frac{\Gamma(t)}{\Gamma} = 1 - \frac{2}{\pi^2}\sum_{n=0}^{\infty}\frac{e^{\left(-\pi^2\left(n+\frac{1}{2}\right)^2 t/\tau\right)}}{\left(n+\frac{1}{2}\right)^2}. \tag{5}$$

$\Gamma$ denotes the surface excess as $t/\tau \to \infty$. In order to describe the experimental data, we need to assume a proportionality between the change in resistance $\Delta R_i$ of the device and the surface excess of analyte, $\Gamma$. We also include the background resistance in synthetic air, $R_0$ to obtain equation (6). The ranges $t_i \leqslant t < t_i$ denote the time periods when the sensor is exposed to analyte and the ranges $t_i \leqslant t < t_{i+1}'$ denote recovery periods when the device is exposed to pure synthetic air.

$$\begin{aligned} R(t) &= R_0 + \Delta R_i\frac{\Gamma(t)}{\Gamma} \qquad t_i \leqslant t < t_i' \\ R(t) &= R_0 + \Delta R_i\left[1 - \frac{\Gamma(t)}{\Gamma}\right] t_i \leqslant t < t_{i+1}'. \end{aligned} \tag{6}$$

The response time of the sensor to a given analyte is determined by a single parameter $\tau = \frac{L^2}{D}$. Equations (5) and (6) define the regression model, which was fitted to the experimental data of figure 9 by the method of least squares. It is worth noting that the response to each analyte is characterised by the same value of $\tau$ as the recovery of the sensor when the analyte stream is replaced by pure synthetic air and the resistance returns towards the baseline.

Table 2 shows a relatively weak variation of response time amongst the four analytes, which is compatible with a diffusion model for this selection of small organic molecules of broadly similar size.

*3.3.2. A kinetic model of the response time of the sensor.* Previous workers have developed a model for situations where the sensor response due to adsorption of the analyte is kinetically-controlled [50]. In this case, the time-dependence is determined by the rate constant for adsorption $k$ and the equilibrium constant $K$ for the adsorption process:

$$A + \theta \rightleftharpoons A.\theta. \tag{7}$$

$A$ is the analyte, $\theta$ is an unoccupied binding site on the surface and $A.\theta$ is an occupied binding site of surface coverage $\Gamma(t)$. The rate of the adsorption process is given by a pseudo-first order law as $kp(\Gamma - \Gamma(t))$ and the rate of the desorption process is given by a first order law as $(kp^{\ominus}/K)\Gamma(t)$. $p$ is the partial pressure of the analyte, $p^{\ominus} = 1$ bar is the standard pressure, $K$ is the dimensionless equilibrium constant for adsorption and $K/p^{\ominus}$ is equal to the ratio of the adsorption and desorption rate constants. The time-dependence of the surface coverage has previously been shown to be simply the difference in the adsorption and desorption rates [50]. In our notation it is given by

**Table 2.** Response times, $\tau$, for the data of figure 9. The values are reported as mean ± estimated standard error. The DNA/MWCNT film was 67% by mass DNA.

| Analyte | $\tau$/s |
|---|---|
| Methanol | $65.3 \pm 4.8$ |
| Ethanol | $72.3 \pm 6.2$ |
| Acetone | $86.8 \pm 9.7$ |
| Chloroform | $108 \pm 11$ |

equation (8)

$$\dot{\Gamma(t)} = kp\Gamma - k\left(p + \frac{p^{\ominus}}{K}\right)\Gamma(t). \tag{8}$$

Equation (8) can also be used to model the experimental data. The quality of the fit is similar to equation (5), because the exponential function, which is the solution of the kinetic equation, provides an equivalent regression model to that obtained by retaining only the first term of the sum in equation (5).

In the recovery experiments, the partial pressure of the analyte $p = 0$ and therefore the recovery rate is determined solely by the rate constant for desorption of the analyte, $kp^{\ominus}/K$. It is therefore necessary, in a kinetic model of the response, to also assume $Kp^{\ominus} \ll p$, which corresponds to very weak binding, in order to explain why the recovery rate is the same as the response rate in the experimental data. Although the data of figure 6 alone is not sufficient to choose between the transport and kinetic models, we favour the former to analyse the device in this work because the analysis of the temperature-dependence of the steady-state response below shows widely varying enthalpies of adsorption for the four analytes (table 5 below). The desorption rates obtained using a kinetic regression model would be proportional to the parameter $\frac{1}{\tau}$ and would be expected to depend on the enthalpy of adsorption in a similar manner to Arrhenius' law. However, the values of $\tau$ vary by less than a factor of 2 and do not show the trend expected for desorption kinetics.

### *3.4. Steady-state sensing response*

The response of individual devices, and their baseline resistance $R_0$, may vary and therefore we discuss the fractional change in resistance $S$ as a function of analyte, partial pressure and temperature. Below $R$ denotes the steady-state resistance as $\Gamma(t) \rightarrow \Gamma$

$$S = 100\% \times \frac{R - R_0}{R_0}. \tag{9}$$

This definition of the analytical signal normalises the raw data so that different devices can be compared.

The dependence of the sensing response on the partial pressure of analyte vapour, $p$ can be modelled on the basis that the normalised signal, $S = \frac{\Delta R}{R_0}$, is proportional to the amount of analyte adsorbed, i.e. the surface concentration $\Gamma$,

$$S = \alpha\Gamma, \tag{10}$$

which in turn is related to $p$ by a model adsorption isotherm.

$$\frac{\Gamma}{\Gamma_m} = \frac{K(p/p^{\ominus})}{1 + K(p/p^{\ominus})}. \tag{11}$$

Equation (11) is the Langmuir isotherm and contains two parameters, $K$ is the equilibrium constant for adsorption and $\Gamma_m$ is the maximum surface excess corresponding to a molecular monolayer of adsorbate. $p^{\ominus} = 1$ bar is the pressure in the thermodynamic standard state. As long as $\Gamma \ll \Gamma_m$ then the signal is proportional to the analyte partial pressure.

Figure 10 shows calibration plots of $S$ against $p/p^*$ for bare MWCNTs and DNA/MWCNT composites of composition 67% and 83% DNA by mass. In general the plots are linear with coefficients of determination >0.9 in most cases (table 3). The analytical sensitivity of these devices is the slope of these plots, $p^*\frac{\partial S}{\partial p}$; the values are collected in table 4. This data indicates that bare MWCNTs have a sensitivity to all the VOCs tested that is of the same order of magnitude, however they are slightly more sensitive to acetone and methanol. In contrast, the DNA/MWCNT composites show a marked selectivity for methanol and in both cases the sensitivity of the devices follows the same order, methanol > ethanol > acetone > chloroform. The large increase in sensitivity of the devices containing DNA over the pure MWCNT device is evidence for the important role played by the DNA molecules in the sensing mechanism. Typical sensing mechanisms based on charge injection from the analyte are not consistent with these observations. Instead, bearing in mind the effect of DNA on the conductance of the DNA/MWCNT composites (figure 8), we suggest that the inter-tube junction resistance is the source of the analytical signal. The sensitivity correlates with established measures of polarity: (i) the relative permittivity of the VOCs as bulk liquids and (ii) their relative polarity assessed from solvatochromic shifts in optical absorption spectra. The DNA/MWCNT composites show higher sensitivity to the more polar analytes as would be expected for the interaction of polar molecules with the charged phosphodiester backbone of DNA.

Figure 11 shows a schematic illustration of our proposed mechanism for the sensing of VOCs by DNA/MWCNT composites. The DNA coating on the MWCNTs increases the tunneling barrier between nanotubes as indicated by the conductance-temperature data of figure (8). Absorption of VOC in the junction region modulates the tunneling barrier further and is responsible for the analytical signal. Similar mechanisms have been observed previously in CNT composites [16, 17].

The nature of the interaction of the analytes with the composites was further investigated by temperature-dependent measurements of the signal. The Dreschel bottle temperature $T'$ was kept constant to control the saturated vapour pressure of the analyte, but the temperature $T$ of the glass cell containing the sensor was controlled by a water bath. The signal $S$ was observed to decrease with an increase in temperature for both 67% DNA/MWCNT composites (figure 12) and bare MWCNTs (figure 13).

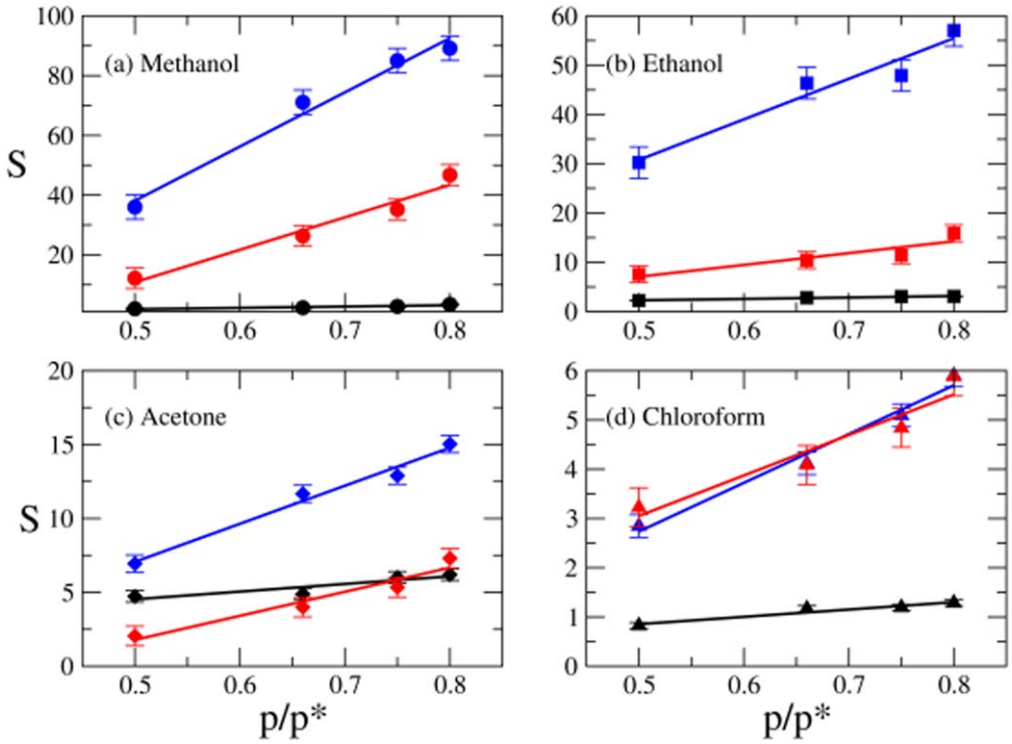


**Figure 10.** Analytical signal against analyte partial pressure as a fraction of the saturated vapour pressure for (a) methanol; (b) ethanol; (c) acetone and (d) chloroform. The percentage by mass of DNA in the composite is indicated by the colour: bare MWCNTs (black), 67% (blue) and 83% (red). The temperature was 17 °C.

**Table 3.** Coefficients of determination ($r^2$) for the calibration plots of figure 10. The percentage by mass of DNA in each composite is indicated.

| Analyte | Bare MWCNTs | 67% DNA/ MWCNT | 83% DNA/ MWCNT |
|---|---|---|---|
| Methanol | 0.848 | 0.981 | 0.962 |
| Ethanol | 0.974 | 0.945 | 0.837 |
| Acetone | 0.817 | 0.981 | 0.939 |
| Chloroform | 0.937 | 0.980 | 0.918 |

This and the low temperatures involved rule out a mechanism based on chemical reactions that require thermal activation, such as charge injection by oxidation of the analyte. The data is however consistent with the adsorption mechanism illustrated in figure 11 or condensation of the analyte on the device.

A model for the temperature dependence of the sensing mechanism can be constructed by choosing a suitable adsorption isotherm. Previous workers have used the Langmuir isotherm [20, 50, 52–54] or Hill's modification [30]. This accounts for specific interactions of the analyte with the composites, but does not account for the possibility of condensation of the vapour on the device as a liquid film. To test this additional possibility, we employ the BET adsorption isotherm, equation (12), which relates the amount of adsorbed analyte to the equilibrium constant $K$ for adsorption at the surface and the saturated vapour pressure, $p^*$

$$\frac{\Gamma}{\Gamma_m} = \frac{K(p/p^{\ominus})}{(1 - p/p^*)(1 + K(p/p^{\ominus}) - p/p^*)}. \tag{12}$$

In equation (12) $p$ is the partial pressure of the analyte and $p^{\ominus}$ is the standard pressure of 1 bar. $\Gamma_m$ is the surface concentration of analyte that comprises a single molecular monolayer. Under the assumption of equation (10), that the signal is proportional to $\Gamma$, the temperature dependence of the sensor signal is then given by equation (13).

$$R\frac{\partial \ln S}{\partial 1/T} = -\Delta H^{\ominus}_{ads} + \Delta H^{\ominus}_{v}\frac{p/p^*}{1 - p/p^*} + \frac{K(p/p^{\ominus})\Delta H^{\ominus}_{ads} + (p/p^*)\Delta H^{\ominus}_{v}}{1 + K(p/p^{\ominus}) - p/p^*}, \tag{13}$$

where the standard enthalpy of adsorption $\Delta H^{\ominus}_{ads}$ and the standard enthalpy of vaporization $\Delta H^{\ominus}_{v}$ are defined by equations (14) and (15). Note that in equations (13)–(17) $R$ is the gas constant and not resistance

$$\frac{\partial \ln K}{\partial 1/T} = -\frac{\Delta H^{\ominus}_{ads}}{R} \tag{14}$$

**Table 4.** Dimensionless analytical sensitivity $\left(p^*\frac{\partial S}{\partial p}\right)$ and the associated standard errors for the calibration plots of figure 10. $\epsilon_r$ is the relative permittivity of the bulk liquid at 298 K and RP is the relative polarity based on solvent shifts in optical absorption spectra [51]. The percentage by mass of DNA in each composite is indicated.

| Analyte | Bare MWCNTs | 67% DNA/CNT | 83% DNA/CNT | $\epsilon_r$ | RP |
|---|---|---|---|---|---|
| Methanol | $4.38 \pm 1.3$ | $182 \pm 18$ | $108 \pm 15$ | 32.7 | 0.762 |
| Ethanol | $2.92 \pm 0.34$ | $82.3 \pm 14$ | $24.0 \pm 7.5$ | 24.55 | 0.654 |
| Acetone | $5.17 \pm 1.7$ | $25.7 \pm 2.6$ | $16.3 \pm 2.9$ | 20.7 | 0.355 |
| Chloroform | $1.49 \pm 0.27$ | $9.89 \pm 1.0$ | $8.21 \pm 1.7$ | 4.81 | 0.259 |

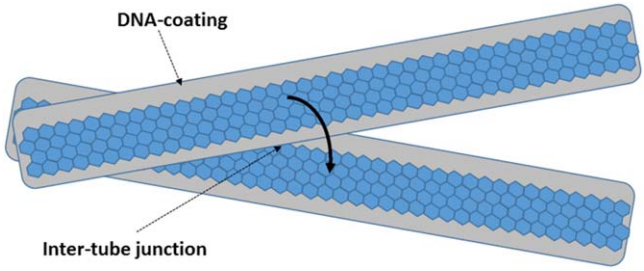


**Figure 11.** Schematic illustration of the junction formed between two DNA-coated carbon nanotubes crossing in the DNA/MWCNT composites. The curved arrow indicates the thermally-activated tunneling process by which charge transfers between nanotubes.

$$\frac{\partial \ln p^*}{\partial 1/T} = -\frac{\Delta H_v^{\ominus}}{R}. \tag{15}$$

In general $\Delta H_{ads}^{\ominus} < 0$ and $\Delta H_v^{\ominus} > 0$. Equation (13) simplifies in two cases. The first corresponds either to the Langmuir isotherm where condensation is negligible or where condensation of the analyte occurs, but has no direct effect on the signal. Dropping terms in $p/p^*$ results in equation (16)

$$\frac{\partial \ln S}{\partial 1/T} = \frac{1}{1 + K(p/p^{\ominus})}\frac{\partial \ln K}{\partial 1/T} \simeq -\frac{\Delta H_{ads}^{\ominus}}{R}. \tag{16}$$

The second case describes the situation where condensation of the analyte as a liquid film dominates the device response, equation (17)

$$\frac{\partial \ln S}{\partial 1/T} = 2\frac{\Delta H_v^{\ominus}}{R}\frac{p/p^*}{1 - p/p^*}. \tag{17}$$

We can distinguish these two cases by the dependence of the apparent enthalpy $\Delta H = -R\frac{\partial \ln S}{\partial 1/T}$ on the analyte partial pressure. In the first case, the apparent enthalpy is weakly decreasing with partial pressure, but in the second case, the apparent enthalpy becomes large and negative as $p/p^* \to 1$.

Figure 14 shows plots of apparent enthalpy against the analyte partial pressure as a fraction of its saturated vapour pressure. The measurements shown in this figure are designed to distinguish the two cases described above. In all datasets, except those of acetone and chloroform on 83% DNA/MWCNTs at low pressure, the apparent enthalpy is roughly constant; this is consistent with a Langmuir model of adsorption and not with condensation of bulk liquid. The green lines in figure 14 show the prediction of equation (17) based on the known enthalpies of vaporization [33] for methanol [55], ethanol [55], acetone [55] and chloroform [56]. It is clear that none of the data is consistent with the limiting case, represented by equation (17), in which condensation of the analyte on the device is the source of the device response. It is also worth noting that the decrease in apparent enthalpy with vapour pressure predicted by equation (16) in the case $Kp/p^{\ominus} > 1$ does not apply either, except in the case of chloroform on 83% DNA/MWCNTs. The other devices are therefore operating in a regime of the isotherm where $\Gamma \propto p$. This is also consistent with the linear calibration plots of figure 10.

Table 5 presents the mean values of the apparent enthalpy averaged over the vapour pressure range investigated. In general, the enthalpy of adsorption of the alcohols on bare MWCNTs is lower than that on the DNA/MWCNT composites, but comparable in the cases of acetone and chloroform. This suggests the origin of the selectivity is related to the interaction of the polar, protic molecules with the polyelectrolyte, DNA.

## 4. Conclusions

DNA and other polyelectrolytes have been used previously to stabilise aqueous dispersions of CNTs. They also modulate the sensing response of nanotubes to organic vapours. We have investigated the conductance and the mechanism of the sensing response of MWCNT/DNA composites prepared by drop-casting aqueous dispersions onto MBEs. Methanol, ethanol, acetone and chloroform were used as test analytes.

Two-terminal current–voltage measurements indicate that increasing the ratio of DNA:CNTs reduces the conductance of the composite and changes the temperature dependence from a metal-like response of bare MWCNTs, in which the conductance decreases with temperature, to an activated behaviour in which the conductance increases with temperature. The temperature-dependence could be fitted with a simple model of two series resistances. The first depends linearly on temperature and models the behaviour of the MWCNTs and the second has the stretched exponential form $\exp\left(\frac{T_0}{T}\right)^{\beta}$ which models the tunneling barriers between nanotubes. As the mole fraction of DNA increases, $T_0$ increases and the second term dominates. It is also possible to choose a composition (3.1% mole fraction, 67% mass fraction of DNA) in which the two opposing temperature dependences compensate and the conductance shows less than 5% change over the range 293–373 K;

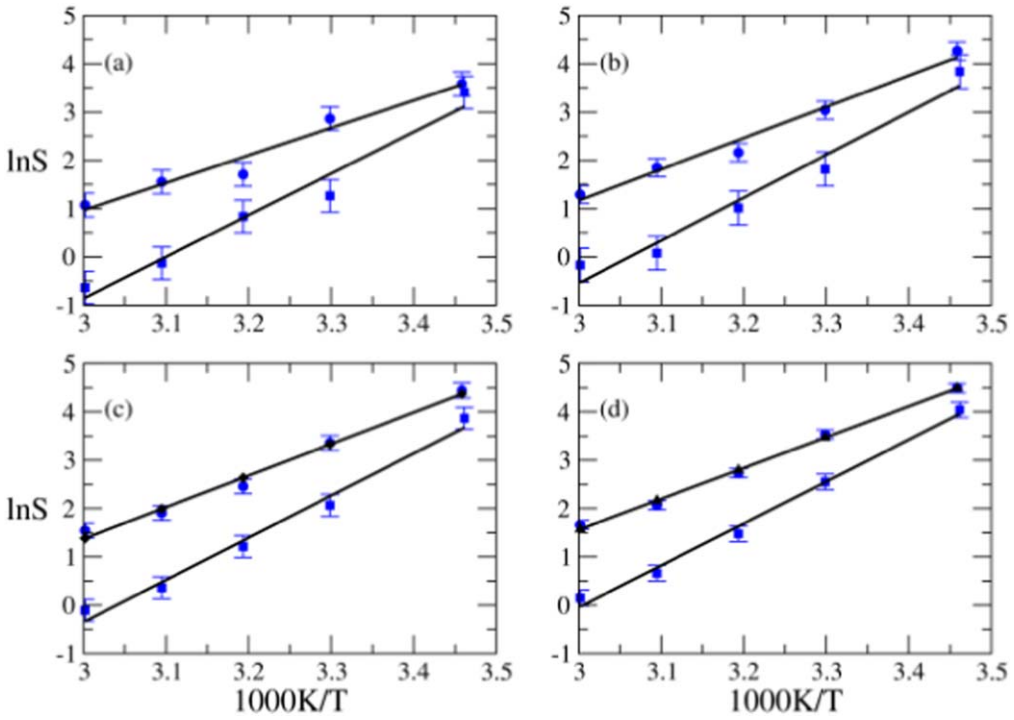


**Figure 12.** ln $S$ against $\frac{1}{T}$ for methanol (circles) and ethanol (squares) on a DNA/MWCNT composite containing 67% DNA by mass. (a) $p/p^*(T') = 0.5$; (b) $p/p^*(T') = 0.66$; (c) $p/p^*(T') = 0.75$; (d) $p/p^*(T') = 0.8$.

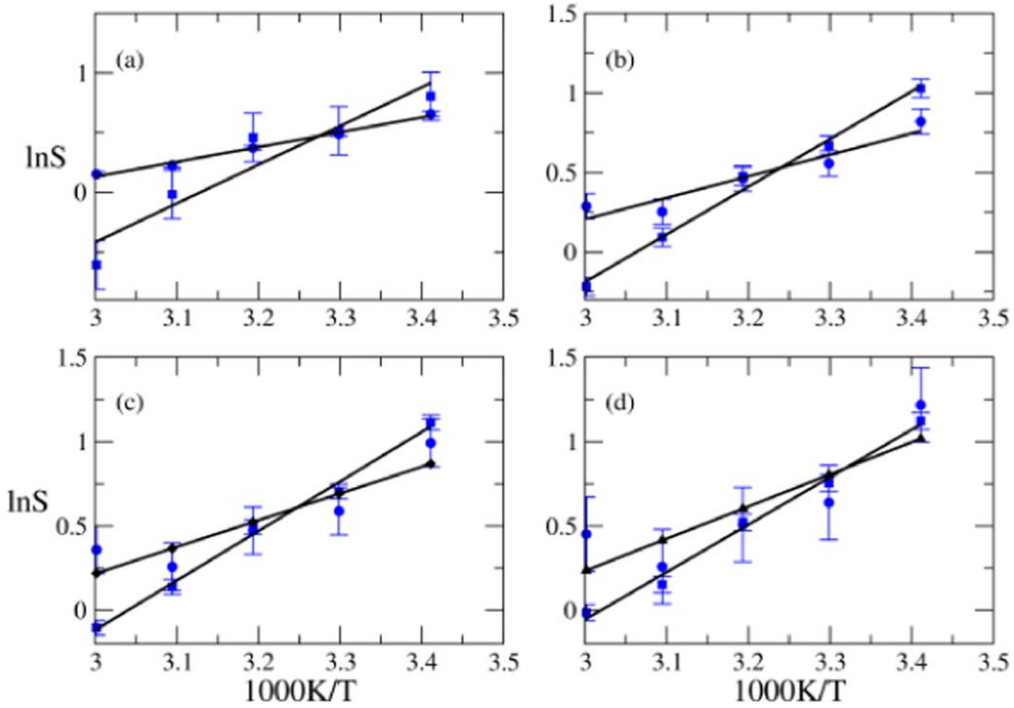


**Figure 13.** ln $S$ against $\frac{1}{T}$ for methanol (circles) and ethanol (squares) on bare MWCNTs. (a) $p/p^*(T') = 0.5$; (b) $p/p^*(T') = 0.66$; (c) $p/p^*(T') = 0.75$; (d) $p/p^*(T') = 0.8$.

this composition is useful for sensing applications in order to discriminate against temperature changes.

Upon exposure of the DNA/MWCNT composites to organic vapours in a flow system with synthetic air as the carrier gas, the resistance of the devices increases. The time-dependence of the resistance change was modelled as a diffusion process in which the analyte penetrates the DNA/MWCNT film. A kinetically-limited adsorption process was found to be unlikely

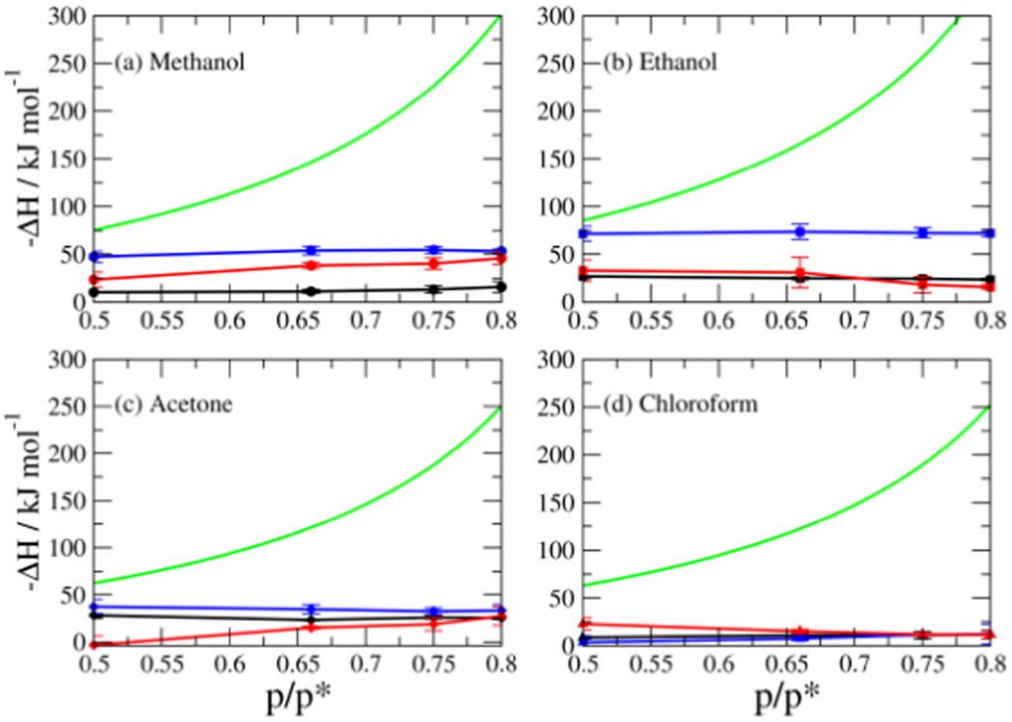


**Figure 14.** Apparent enthalpy $-\Delta H = R\frac{\partial lnS}{\partial 1/T}$ against partial pressure $p/p^*(T')$. The green lines show the predictions of equation (17) for condensation of the analyte on the device. Experimental data for (black) bare MWCNTs, (blue) 67% DNA/MWCNTs and (red) 83% DNA/MWCNTs.

**Table 5.** Mean apparent enthalpies of adsorption $\overline{\Delta H}$/kJ mol$^{-1}$ determined from the temperature dependence of the sensing response. The percentage by mass of DNA is indicated for each composite.

| Analyte | Bare MWCNTs | 67% CNT/DNA | 83% CNT/DNA |
|---|---|---|---|
| Methanol | $-12.7 \pm 3.0$ | $-52.2 \pm 4.0$ | $-36.9 \pm 5.9$ |
| Ethanol | $-24.9 \pm 2.3$ | $-72.5 \pm 6.2$ | $-24.5 \pm 9.5$ |
| Acetone | $-25.7 \pm 1.5$ | $-34.4 \pm 5.7$ | $-14.5 \pm 6.9$ |
| Chloroform | $-10.6 \pm 3.6$ | $-8.8 \pm 4.8$ | $-15.3 \pm 3.3$ |

because the recovery of the resistance after exposure to analyte does not correlate with the enthalpy of adsorption in the manner expected for a desorption rate constant.

The fractional change in the device resistance at steady-state upon exposure to analyte was used as a sensing signal. Linear calibration plots were observed for all the devices prepared, but the sensitivity of the DNA/MWCNT composites was greater than that of the bare MWCNT device, although increasing the amount of DNA does not result in progressively greater sensitivity. The incorporation of DNA also shifted the selectivity of the devices in favour of the most polar analytes. The data can be described satisfactorily by a model in which analyte adsorption in the DNA-coated nanotube junctions modulates the inter-tube resistance. Temperature-dependent sensing measurements were satisfactorily described by a simple model based on the Langmuir adsorption isotherm and the proportionality of the signal to the amount of analyte adsorbed. The analysis of this data showed that condensation of VOCs on the device as liquid films does not affect the response of the device, but the measured adsorption enthalpies of the analytes indicates stronger interaction of the polar, protic species with the composites.

## Acknowledgments

Jake Sheriff and Lidija Šiller are thanked for the XPS measurements at NEXUS, Newcastle University. The Electron Microscopy and Analysis Unit at SAgE Analytical, Newcastle University is thanked for the scanning electron microscopy.

## Data availability statement

The data that support the findings of this study are available upon reasonable request from the authors.

## ORCID iDs

Shams B Ali https://orcid.org/0000-0003-0232-7341
Andrew Houlton https://orcid.org/0000-0001-5633-4630
Benjamin R Horrocks https://orcid.org/0000-0001-7047-2319

## References


[1] Dresselhaus M S, Dresselhaus G and Eklund P C 1996 *Science of Fullerenes and Carbon Nanotubes* (San Diego, CA: Academic)
[2] Haddon R C 2002 *Acc. Chem. Res.* **35** 997–1113
[3] Swager T M 1998 *Acc. Chem. Res.* **31** 201–7
[4] Kauffman D R and Star A 2008 *Angew. Chem. Int. Ed. Engl.* **47** 6550–70
[5] Schroeder V, Savagatrup S, He M, Lin S and Swager T M 2019 *Chem. Rev.* **119** 599–663
[6] Kong J, Franklin N R, Zhou C, Chapline M G, Peng S, Cho K and Dai H 2000 *Science* **287** 622–5
[7] Tans S J, Verschueren R M and Dekker C 1998 *Nature* **393** 49–52
[8] Martel R, Schmidt T, Shea H R, Hertel T and Avouris P 1998 *Appl. Phys. Lett.* **73** 2447–9
[9] Collins P G, Bradley K, Ishigami M and Zettl A 2000 *Science* **287** 1801–4
[10] Boyd A, Dube I, Fedorov G, Paranjape M and Barbara P 2014 *Carbon* **69** 417–23
[11] Heller I, Janssens A M, Männik J, Minot E D, Lemay S G and Dekker C 2008 *Nano Lett.* **8** 591–5
[12] Bondavalli P, Legagneux P and Pribat D 2009 *Sensors Actuators* B **140** 304–18
[13] Peng G, Tisch U and Haick H 2009 *Nano Lett.* **9** 1362–8
[14] Ponnamma D, Sadasivuni K K, Strankowski M, Guo Q and Thomas S 2013 *Soft Matter* **9** 10343–53
[15] Salehi-Khojin A, Khalili-Araghi F, Kuroda M A, Lin K Y, Leburton J P and Masel R I 2011 *ACS Nano* **5** 153–8
[16] Li C, Thostenson E T and Chou T W 2007 *Appl. Phys. Lett.* **91** 223114
[17] Hu N, Karube Y, Yan C, Masuda Z and Fukunaga H 2008 *Acta Mater.* **56** 2929–36
[18] Wei C, Dai L, Roy A and Tolle T B 2006 *J. Am. Chem. Soc.* **128** 1412–3
[19] Wang H C, Li Y and Yang M J 2007 *Sensors Actuators* B **124** 360–7
[20] Qi P, Vermesh O, Grecu M, Javey A, Wang O, Dai H J, Peng S and Cho K J 2003 *Nano Lett.* **3** 347–51
[21] Zheng M, Jagota A, Semke E D, Diner B A, Mclean R S, Lustig S R, Richardson R E and Tassi N G 2003 *Nat. Mater.* **2** 338–42
[22] Zheng M *et al* 2003 *Science* **302** 1545–8
[23] Asada Y, Miyata Y, Ohno Y, Kitaura R, Sugai T, Mizutani T and Shinohara H 2010 *Adv. Mater.* **22** 2698–701
[24] Wang R, Sun J, Gao L and Zhang J 2010 *J. Mater. Chem.* **20** 6903–9
[25] Wang Y, Liu H, Wang F and Gao Y 2012 *J. Solid State Electrochem.* **16** 3227–35
[26] Tang X, Bansaruntip S, Nakayama N, Yenilmez E, Chang Y L and Wang Q 2006 *Nano Lett.* **6** 1632–6
[27] Staii C, Johnson A T, Chen M and Gelperin A 2005 *Nano Lett.* **5** 1774–8
[28] Johnson A T C, Staii C, Chen M, Khamis S, Johnson R, Klein M L and Gelperin A 2006 *Semicond. Sci. Technol.* **21** S17–21
[29] Khamis S M, Jones R A, Johnson A T C, Preti G, Kwak J and Gelperin A 2012 *AIP Adv.* **2** 022110
[30] Kybert N J, Lerner M B, Yodh J S, Preti G and Johnson A T C 2013 *ACS Nano* **7** 2800–7
[31] Sanger F, Coulson A R, Hong G F, Hill D F and Petersen G B 1982 *J. Mol. Biol.* **162** 729–73
[32] Fairley N *et al* 2021 *Appl. Surf. Sci. Adv.* **5** 100112
[33] Acree W E Jr and Chickos W G 2020 Phase transition enthalpy measurements of organic and organometallic compounds *NIST Chemistry Webbook* ed P Linstrom and J S Mallard (Gaithersburg MD: National Institute of Standards and Technology) p 20899 NIST Standard Reference Database Number 69
[34] Storm A J, van Noort J, de Vries S and Dekker C 2001 *Appl. Phys. Lett.* **79** 3881–3
[35] Bockrath M, Markovic N, Shepard A, Tinkham M, Gurevich L, Kouwenhoven L P, Wu M W and Sohn L L 2002 *Nano Lett.* **2** 187–90
[36] Gomez-Navarro C, Moreno-Herrero F, de Pablo P J, Colchero P J, Gómez-Herrero J and Baró A M 2002 *Proc. Natl. Aacd. Sci. USA* **99** 8484–7
[37] Sonmezoglu S, Sonmezoglu O A, Cankaya G, Yildirim A and Serin N 2010 *J. Appl. Phys.* **107** 124518
[38] Umemura K 2015 *Nanomaterials* **5** 321–50
[39] Okpalugo TITand Papakonstantinou P, Murphy H, McLaughlin J and Brown N 2005 *Carbon* **43** 153–61
[40] Aleman B, Vila M and Vilatela J J 2018 *Phys. Status Solidi* A **215** 18000187
[41] Gottardi G, Laidani N, Bartali R, Micheli V and Anderle M 2008 *Thin Solid Films* **516** 3910–8
[42] Mateo-Martí E, Briones C, Pradier C and Martín-Gago J A 2007 *Biosens. Bioelectron.* **22** 1926–32
[43] Petrovykh D Y, Kimura-Suda H, Whitman L J and Tarlov M J 2003 *J. Am. Chem. Soc.* **125** 5219–26
[44] Erfurth S C and Peticolas W L 1975 *Biopolymers* **14** 247–64
[45] Benvenides J M and Thomas G J Jr 1983 *Nucleic Acids Res.* **11** 5747–61
[46] Ouameur A A and Tajmir-Riahi H A 2004 *J. Biol. Chem.* **279** 42041–54
[47] Alex S and Dupuis P 1989 *Inorg. Chim. Acta* **157** 271–81
[48] Dovbeshko G I, Gridina N Y, Kruglova E B and Pashchuk O P 2000 *Talanta* **53** 233–46
[49] Sheng P, Abeles B and Arie Y 1973 *Phys. Rev. Lett.* **31** 44–7
[50] Lee C Y and Strano M S 2005 *Langmuir* **21** 5192–6
[51] Reichardt C and Welton T 2011 *Solvents and Solvent Effects in Organic Chemistry* 4th edn (New York: Wiley)
[52] Wongwiriyapan W *et al* 2005 *Japan. J. Appl. Phys.* **44** 482–4
[53] Robinson J A, Snow E S, Badescu S C, Reinecke T L and Perkins F K 2006 *Nano Lett.* **6** 1747–51
[54] Battie Y, Ducloux O, Thobois P, Dorval N, Lauret J S, Attal-Trétout B and Loiseau A 2011 *Carbon* **49** 3544–52
[55] Majer V and Svoboda V 1985 *Enthalpies of Vaporization of Organic Compounds: A Critical Review and Data Compilation* (Oxford: Blackwell Scientific Publications)
[56] Stephenson R M and Malanowski S 1987 *Handbook of the Thermodynamics of Organic Compounds* (Dordrecht: Springer)